Research article

X-RAY SPECTROMETRY

Received: 22 November 2016 Revised: 28 April 2017 Accepted: 1 May 2017 Published online in Wiley Online Library

(wileyonlinelibrary.com) DOI 10.1002/xrs.2782

Quantitative speciation of manganese oxide mixtures by RIXS/RRS spectroscopy

Juan José Leani,[a,b]* José Ignacio Robledo[a,b] and Héctor Jorge Sánchez[a,b]

Resonant inelastic X-ray scattering, also named X-ray resonant Raman scattering, was recently used to discriminate local chemical environments. By means of this novel technique, the speciation of samples could be attained in a variety of samples and experimental conditions. Until now, this discrimination methodology had been applied only to pure compounds, being the speciation possible by two different mathematical treatments. Nevertheless, the effectiveness/sensitivity of this technique has not been tested yet in samples containing mixtures of oxides of the same element. In this work, the first results of quantitative speciation of mixtures of manganese compounds, using resonant inelastic X-ray scattering/X-ray resonant Raman scattering spectroscopy, are presented. The results show that it is possible to discriminate and quantify oxide mixtures of the same element in slightly different proportions, allowing a quantitative speciation of compound mixtures in a variety of experimental conditions, presenting also several advantages over conventional spectroscopic techniques. Copyright © 2017 John Wiley & Sons, Ltd.

Introduction

In material science, the study of alloys is very important because they have properties that can differ in great manner from those of their composing elements. Alloying elements are added to base metals to enhance some particular properties as hardness, strength, corrosion resistance, electrical and magnetic properties, etc. Such enhancement properties make them more useful and tunable for particular demands. While some alloys are found in nature, such as electrum (a mix of silver and gold) or meteoric iron–nickel, humans have been creating alloys for their own use for more than 4500 years. An early example of a fabricated alloy is bronze, which is made from copper and tin, being harder and stronger than those pure elements. Another very common example is steel, harder and tougher than pure iron. Because of their properties, metal alloys can be successfully adapted to specific uses where a pure metal would be either unsuitable or extremely expensive.

A relevant element in alloys is manganese. This element is present in several metal mixtures, and because of its particular characteristics, manganese has no satisfactory substitute in its major applications in metallurgy.[1] Manganese is, for example, essential for iron and steel production by virtue of its sulfur-fixing, deoxidizing, and alloying properties. Small amounts of manganese improve the workability of steel at high temperatures by forming a high-melting sulfide and preventing the formation of a liquid iron sulfide at the grain boundaries. Steel with 1.5% Mn and 0.25% C is a cheaper steel, used for car axles and crankshafts. Steel with 1.5% of Mn and 0.35% of C is used in automobiles and general engineering in situations where the expense of Ni–Cr steel is not justified. If the manganese content reaches 4%, the embrittlement of the steel becomes a dominant feature. The embrittlement decreases at higher manganese concentrations and reaches an acceptable level at 8%. Steel containing 8 to 15% of manganese has a high tensile strength of up to 863 MPa.[2,3] Hadfield steel is the classic manganese alloy steel with more than 12% of Mn; it is used in situations where toughness combined with extreme abrasion resistance is required, as rock crushing machinery, dredging equipment, and track work points and crossings. Hadfield steel was used as for the British military for helmets and later by the US army.[4] In addition, silico-manganese (heating oxides MnO_2 SiO_2, and Fe_2O_3 with carbon) has applications as deoxidizer and an alloying element in steel as well; aluminum with roughly 1.5% manganese has increased resistance to corrosion through grains that absorb impurities that would lead to galvanic corrosion, between so many cases and examples. Clearly, the oxidation state of manganese compounds is also important in many fields of science and industry, like agronomy and medicine.[5,6]

It is evident that small variations on the amount of Mn, or in its oxidation state, can produce notable changes on the features of the related alloy compound. That is why a precise characterization of its concentration and chemical state is mandatory for a proper quantification process. Due to its vast use in many fields of the industry, a reliable Mn characterization procedure is of the highest importance.

Resonant inelastic X-ray scattering, also known as resonant Raman scattering (RIXS/RRS), is the basis of a novel and promising X-ray spectrometric technique for the determination of the atomic environment. This methodology is fundamented on an inner shell atomic process involving an incident photon, bound electrons, and a scattered photon. This RIXS/RRS process was observed for the first time by Sparks[7] in 1974 and explained later by Bannet and Freund[8] in 1975. First studies on the K-level cross sections for some transitions elements by using both conventional X-ray sources and synchrotron radiation were published during the seventies and eightees.[7,9–14] Systematic measurements of the total cross section as a function of the incident energy were reported by Sánchez *et al.* in 2006[15] for pure metals and by Valentinuzzi *et al.* in 2008 for oxides.[16] The first report of determining atomic environments by the inspection of the fine structure of the

* *Correspondence to: Juan José Leani, IFEG, National Scientific and Technical Research Council (CONICET), X5000HUA Córdoba, Argentina. E-mail: ljj@famaf.unc.edu.ar*

a *IFEG, National Scientific and Technical Research Council (CONICET), X5000HUA, Córdoba, Argentina*

b *FaMAF, Universidad Nacional de Córdoba (UNC), X5000HUA, Córdoba, Argentina*

RIXS/RRS spectra by using a low resolution system is from 2011 by Leani *et al.*,[17] and the influence of RIXS/RRS on the quantification of XRF analyses was theoretically calculated by Sánchez *et al.*[18] in 2012.

The RIXS/RRS can be observed by using high-energy resolution systems for detecting the scattered photon, which provided a detailed information about the decay process. However, high-energy resolution spectrometers for a wide range of energies are not available and, usually, the measuring time turns unhandled. Most interesting and useful results can be obtained by using low-energy resolution systems. In this configuration, RIXS/RRS experiments are completely equivalent to X-ray fluorescence experiments, including all the different variations of XRF, i.e. total reflection, spatially resolved analysis, and surface analysis by grazing incidence excitation.

In 2013, Leani *et al.*[19] successfully performed a qualitative microanalysis of calcium local structure in tooth layers by means of micro-RIXS/RRS combining for the first time RIXS/RRS and spatially resolved spectroscopy. A depth profiling nanoanalysis of chemical environments using resonant Raman spectroscopy was carried out by Leani *et al.*[20] in 2013 and represented the first experiment of RIXS/RRS at grazing incidence conditions. In addition, total reflection geometry was employed to determine arsenic speciation by RIXS/RRS in 2013.[21]

Until now, this discrimination methodology had been applied only to pure oxides, achieving the speciation by specific mathematical treatments. Nevertheless, the effectiveness of this technique was not tested in samples containing mixtures of oxides of the same element or alloys.

In this work, first results regarding quantitative speciation of manganese compound mixtures by RIXS/RRS spectroscopy are presented. Calibration curves were established, and testing samples were calculated with significant success. The results are discussed, and the sensitivity of the technique is evaluated.

Experimental

The measurements were carried out at the Brazilian Synchrotron Light Source (Campinas) in the D09B-XRF beamline.[22] This beamline is equipped with a double-crystal channel-cut monochromator with energy resolutions of 3 eV and 10 keV using an Si(111) crystal. The measurements for this work were carried out in a typical reflection geometry (45°–45°) in the orbit's plane so as to minimize Compton and Rayleigh scattering contribution.[23] A monochromatic beam was used, setting the incident energy at 6450 eV, i.e. beneath the K absorption edge of manganese. The incident beam flux was of approximately 10^8 ph/s. Outgoing photons were detected with an energy dispersive ultra low-energy germanium solid-state detector with a beryllium window of 8 m and an energy resolution of 140 eV for the Mn–K line.

The samples under analysis were divided into two groups. The first group (group A) consisted of four pellets with Mn_2O_3 and MnO_2 mixed in different proportions: (1) 100% of Mn_2O_3; (2) 80% Mn_2O_3 and 20% MnO_2; (3) 60% Mn_2O_3 and 40% MnO_2; (4) 20% Mn_2O_3 and 80% MnO_2; and (5) 100% MnO_2. The second group (group B) consisted of four mixtures of Mn_2O_3 and MnO also with different amounts of each oxide: (1) 100% of Mn_2O_3; (2) 75% of Mn_2O_3 and 25% of MnO; (3) 25% of Mn_2O_3 and 75% of MnO; and (4) 100% of MnO. Every sample mentioned in the preceding texts had 0.05 g of boron nitrate and weighed a total of 0.2 g of manganese compounds.

In addition, two more samples were measured in order to check the calibration curve for quantification (validation samples). For group A, the sample consisted of 40% Mn_2O_3 and 60% MnO_2, and for group B, the sample consisted of 50% Mn_2O_3 and 50% MnO.

Four spectra were measured for each of the samples of the first group and three spectra for each sample of the second group. In both groups, every spectrum's acquisition live time was of 500 s. An RIXS/RRS spectrum is shown in Fig. 1 [region of interest (ROI) also plotted].

Data analysis and results

The spectrum analysis was approached by two independent mathematical methods: fine structure deconvolution technique[17] and principal component analysis (PCA) technique.[24] These spectral analyses were performed to each group of spectra (A and B) independently.

For the fine structure deconvolution, spectra were treated with specific analysis programs (OriginLab[25] and TableCurve[26]). The data fitting of the low-energy side of the RRS peaks was achieved by means of a Lorentzian decay.[17] After the fitting, a fast Fourier transform smoothing procedure was applied to the residuals, taking into account a Gaussian instrumental function with a σ of 67 eV.

Figure 2 shows the low-energy side residuals between the RRS peak and the Lorentzian fitting (starting just in the peak maximum amplitude) for group A samples (mixtures of Mn_2O_3 and MnO_2 compounds) and Fig. 3 for group B samples (composited by Mn_2O_3 and MnO oxides).

As it can be seen from Figs. 2 and 3, the oscillation pattern present in the RRS residuals of the mixtures seems to be a convolution between the oscillation patterns of the pure constitutive compounds. In order to evaluate and quantify this oscillation pattern mixture, a PCA mathematical procedure was performed to each set of raw data. In this way, the use of the fine-structure method result is avoided in order to study only the nonconvoluted spectral behavior.

Principal component analysis is a multivariate technique that allows the study of the variance–covariance structure of a data set from a mathematical point of view. It successfully disassembles the total variance into smaller components, the principal components, allowing to search through the data set by parts, prioritizing those parts that explain the largest amount of the total variance. It is increasingly used in X-ray spectrometry because of its simplicity and the amount of information that can be understood through it.[27–29]

To perform the PCA in each group of spectra, the RRS tail ROI was separated from each spectrum. This ROI corresponds to 16 energy channels (in both groups of spectra), ranging between 5645 and 5850 eV (Fig. 1). This selection depends mainly on two factors: the number of spectra that we have as input for the PCA (normally called n in multivariate literature) and the presence of any potential peak from strait elements that may interfere with the RRS oscillations (this interference should be excluded from the analysis). Because PCA is a multivariate method that acts upon the covariance matrix, which has dimensions $p \times p$ (where p is the number of variables), it is normally recommended and convenient to have $n > p$. So, as to be able to use a larger set of input variables (in our case the energy channels of the RRS ROI), it is necessary for n to be large. A normalization of each spectrum was required as to eliminate any undesired variability in between spectra, like any

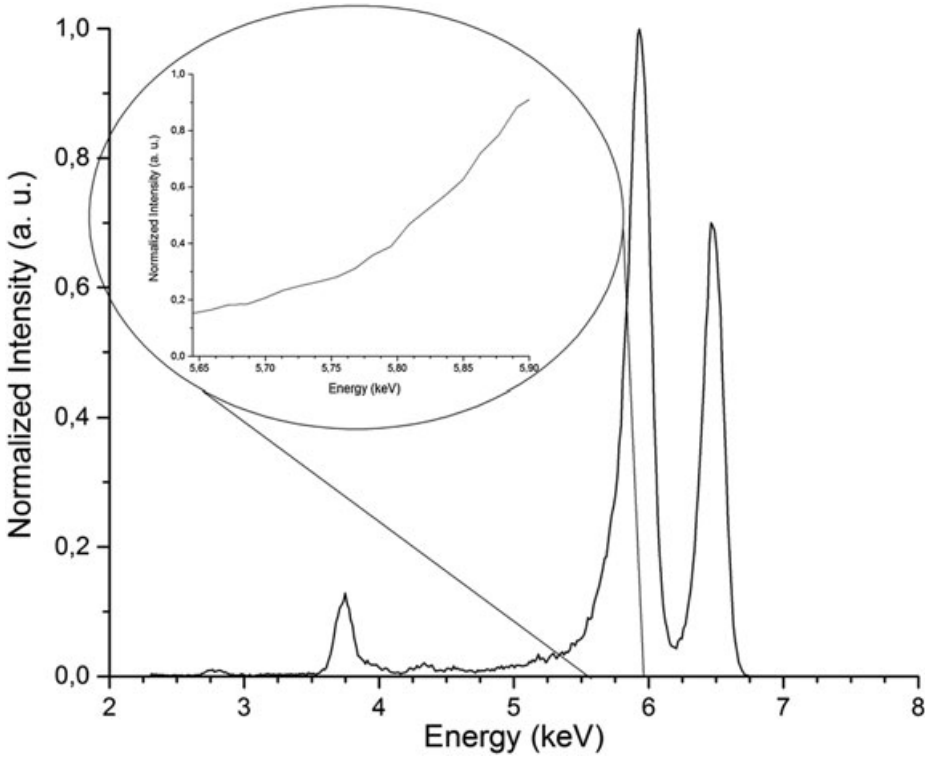

Figure 1. Example of a measured RIXS/RRS spectrum (elastic peak also visible) and inset, the selected ROI for the PCA procedure.

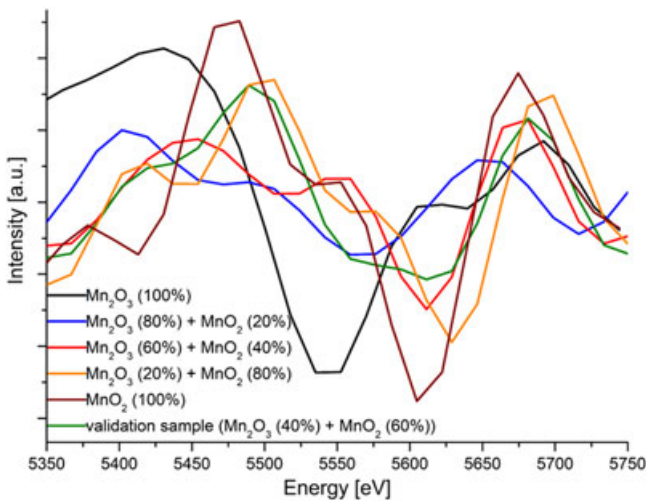

Figure 2. RIXS/RRS low-energy residuals for the samples containing mixtures of Mn_2O_3 and MnO_2 (group A).

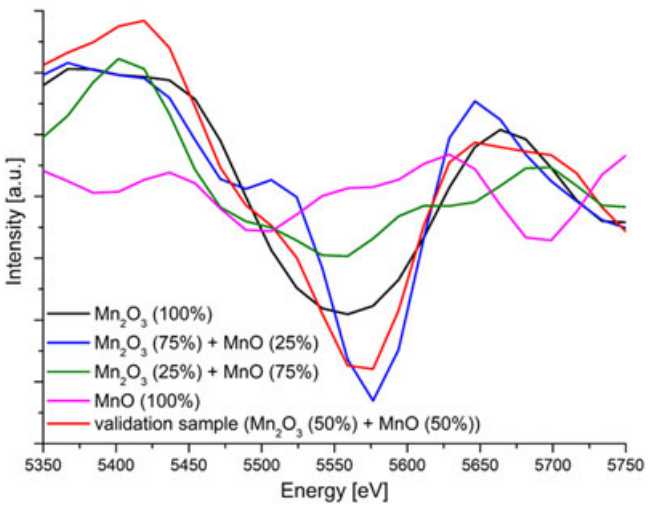

Figure 3. RIXS/RRS low-energy residuals for the samples containing mixtures of Mn_2O_3 and MnO (group B).

variability corresponding to the measuring time, the amount of element of interest in the irradiation volume or any small variation of the flux. This normalization was performed by dividing each spectrum by the amplitude, i.e. the counts on the channel of maximum intensity, of its RRS peak. PCA was performed with InfoStat[30] and cross-checked with a Python subroutine from matplotlib.[31] It is noticed that the spectral shape does not significantly change after some time of acquisition, being convenient then, from a statistic point of view, to have more measurements of shorter acquisition time than only one long measurement.

After PCA was performed, all spectra were projected only onto the first principal component (PC1) because, in both cases, it explained more than half of the total variability of the data set (86% for group A and 56% for group B) and it was sufficient for the discrimination. This means that the variability in the spectra regarding the chemical state was contemplated by this PC and only by this one because PCs are orthogonal. It is worth mentioning that, in both cases, only the first five principal components had nonzero values, and that in both cases, PC1 was by far the most significant one. The projections of all spectra onto this principal component were classified by their corresponding mixture sample. The mean

value of the PC1 projections of spectra belonging to the same sample was calculated. We refer to these sample means as the sample centroids. In this way, we obtained a weight in the PC1 that corresponds to the centroid of spectra belonging to a specific mixture sample. This value of the sample centroid becomes more representative of the population mean if the amount of spectra of the same sample increases. A list of these centroids for the different mixture compounds and their corresponding standard error is given in Table 1. Afterward, these centroids were used to perform a calibration curve (by least squares fitting) with the aim of quantifying the amount of mixture of any unknown sample. Figures 4 and 5 show the calibration curves of PC1 *versus* the concentration of Mn_2O_3 corresponding to groups A and B, respectively. The figures also show the validation samples (empty circle) and the errors of every point (defined as the standard error of each sample distribution in PC1).

Table 2 shows the concentration of the validation samples and the estimated values obtained from the corresponding calibration curves. The errors of the estimated concentrations were calculated by propagation by using partial derivatives.

The results show that different compound mixtures, in this case of manganese, can be successfully discriminated and characterized by using this RIXS/RRS technique. The applied methodology is the typical one for a calibration method, using standards with graduated mixture concentrations. In principle, at least two standards are necessary to calibrate the system and calculate the quantification line. Nevertheless, it is expected that a more accurate calibration curve will be obtained taking into account as many standards as possible.

The mathematical procedure for the calculation of concentrations of any unknown sample is fairly straightforward, based on PCA and on a simple linear fitting.

Regarding the validation samples, the results are quite precise, showing values very close to the actual concentrations (36% instead 40% for sample group A and 49% instead 50% for group B). The propagated errors of the calculated concentrations are relatively high, depending strongly on the standard deviation of the PC1 sample distributions. This indicates that in order to improve the sensitivity of the methodology and reduce the concentration uncertainties, more measurements of shorter acquisition time of the standards are desired.

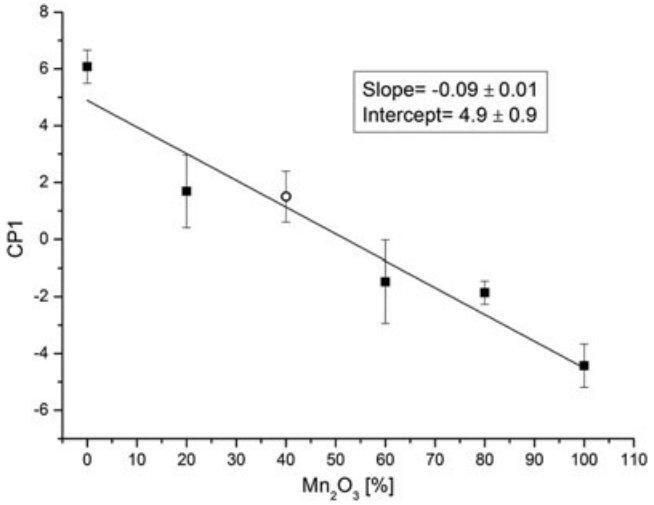

Figure 4. Calibration curve of PC1 centroids *versus* concentration of Mn_2O_3 corresponding to group A. The figure shows the measured calibration points (black squares) and the testing sample (empty circle). Errors of every point are defined as the standard deviation of each PC1 sample distribution.

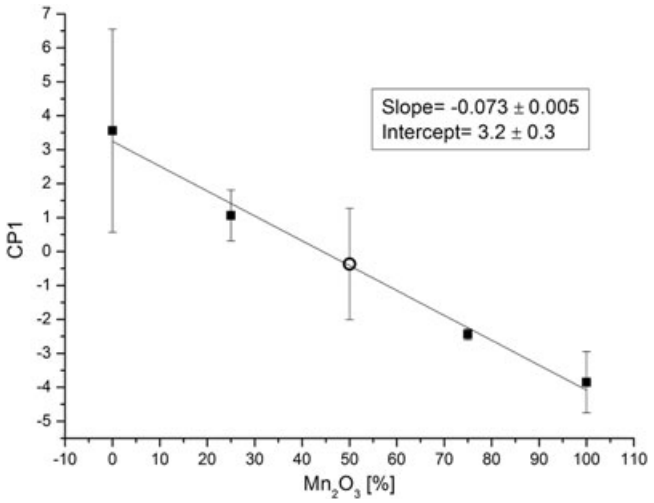

Figure 5. Calibration curve of PC1 centroids *versus* concentration of Mn_2O_3 corresponding to group B. The figure shows the measured calibration points (black squares) and the testing sample (empty circle). Errors of every point are defined as the standard deviation of each PC1 sample distribution.

Table 1. Weight in PC1 of the calculated centroids for the different mixture compounds and their corresponding standard deviations for samples of groups A and B

Group	Mn_2O_3 [%]	Weight in PC1	SD
A	0	6.08	0.58
A	20	1.69	1.28
A	60	−1.48	1.46
A	80	−1.86	0.41
A	100	−4.43	0.76
Validation sample A	40	1.5	0.9
B	0	3.56	2.99
B	25	1.06	0.75
B	75	−2.44	0.16
B	100	−3.85	0.9
Validation sample B	50	−0.37	1.64

Table 2. Concentrations of the validation samples, for groups A and B, and the calculated values obtained from the calibration curves. Errors were calculated by propagation by using partial derivatives.

MMn_2O_3	Concentration [%]	Estimation [%]
Group A	40	36 ± 13
Group B	50	49 ± 22

Conclusions

The application of the novel RIXS/RRS tool in combination with PCA for data analysis shows the capability to discriminate and characterize oxide mixtures of the same element with high sensitivity.

Mixtures of manganese oxides were successfully discriminated by the RIXS/RRS technique. The results exposed in this survey can be extended to other oxides for application in many field of science, as geology, chemistry, physics, etc, and mainly to material science and industry, were a precise quantification of different compounds of the same elements in slightly different proportions is needed.

The whole methodology is fast, simple, and reliable. It presents several advantages compared with other spectroscopic techniques, as fast acquisition, low self-absorption, and the avoidance of any energy scan during the measurements, being even possible then to perform this kind of analysis in a local laboratory by using an X-ray tube with proper anode or secondary target.

Acknowledgements

This work was partially supported by the Brazilian Synchrotron Light Source/CNPEM (Campinas, Brazil).

References

[1] L. A. Corathers, "Mineral commodity summaries 2009: manganese". United States Geological Survey. Retrieved **2009**.
[2] J. H. Stansbie, *Iron and Steel*, Read Books, London, United Kingdom, **2007**, pp. 351–352.
[3] G. S. Brady, H. R. Clauser, J. A. Vaccari, *Materials Handbook: An Encyclopedia for Managers, Technical Professionals, Purchasing and Production Managers, Technicians, and Supervisors*, McGraw-Hill, New York, NY, **2002**, pp. 585–587.
[4] L. Alessio, M. Campagna, R. Lucchini. *Am J Ind Med* **2007**, *50*(11), 779–787.
[5] D. G. Schulze, S. R. Sutton, S. Bajt. *Soil Sci Soc Am J* **1995**, *59*(6), 1540.
[6] S. H. Reaneya, D. R. Smith. *Toxicol Appl Pharmacol* **2005**, *205*(3), 271.
[7] C. J. Sparks. *Phys Rev Lett* **1974**, *33*, 262.
[8] Y. B. Bannet, I. Freund. *Phys Rev Lett* **1975**, *34*, 372.
[9] P. Suortti. *Phys Status Solidi B* **1979**, *91*, 657.
[10] K. Hämäläinen, S. Manninen, P. Suorti, S. P. Collins, M. J. Cooper, D. Laundy. *J Phys Condens Matter* **1989**, *1*, 5955.
[11] J. Tulki, T. Aberg. *J Phys B: At Mol Phys* **1982**, *15*, 435.
[12] J. P. Briand, D. Girard, V. O. Kostroun, P. Chevalier, K. Wohrer, J. P. Moss. *Phys Rev Lett* **1981**, *46*, 1625.
[13] Y. B. Bannett, D. C. Rapaport, I. Freund. *Phys Rev A* **1977**, *16*, 2011.
[14] S. Manninen, P. Suortti, M. J. Cooper, J. Chomilier, G. Loupias. *Phys Rev B* **1986**, *34*, 8351.
[15] H. J. Sánchez, M. C. Valentinuzzi, C. Pérez. *J Phys B* **2006**, *39*, 4317–4327.
[16] M. C. Valentinuzzi, H. J. Sánchez, J. Abraham, C. Pérez. *X Ray Spectrom.* **2008**, *37*, 555.
[17] J. J. Leani, H. J. Sánchez, M. C. Valentinuzzi, C. A. Pérez. *J Anal At Spectrom* **2011**, *26*, 378–382.
[18] H. J. Sánchez, M. C. Valentinuzzi, J. J. Leani. *J Anal At Spectrom* **2012**, *27*, 232.
[19] J. J. Leani, H. J. Sánchez, M. C. Valentinuzzi, C. Pérez, M. Grenón. *J Microsc* **2013**, *250*, 111.
[20] J. J. Leani, H. J. Sánchez, R. D. Pérez, C. Pérez. *Anal Chem* **2013**, *85*, 7069.
[21] H. J. Sánchez, J. J. Leani, R. D. Pérez, C. Pérez. *J Appl Spectrosc* **2013**, *80*, 920.
[22] C. A. Pérez, M. Radke, H. J. Sánchez, H. Tolentino, R. T. Neuenshwander, W. Barg, M. Rubio, M. I. Silveira Bueno, I. M. Raimundo, J. R. Rohwedder. *X Ray Spectrom.* **1999**, *28*, 320.
[23] A. L. Hanson. *Nucl Instrum Meth* **1986**, *243*, 583–598.
[24] J. I. Robledo, H. J. Sánchez, J. J. Leani, C. A. Pérez. *Anal Chem* **2015**, *87*, 3639.
[25] Origin. OriginLab: Northhampton, MA, 2003.
[26] TableCurve v1.11 for Windows. Copyright 1993, AISN Software.
[27] J. B. Ghasemi, K. Rofouei, N. Amiri. *X Ray Spectrom.* **2014**, *43*, 131.
[28] D. Di Giuseppe, G. Bianchini, B. Faccini, M. Coltorti. *X Ray Spectrom* **2014**, *43*, 165.
[29] J. B. Ghasemi, M. K. Rofouei, N. Amiri. *X Ray Spectrom.* **2015**, *44*, 75.
[30] M.G. Balzarini, L. González, M. Tablada, F. Casanoves, J.A. Di Rienzo, C.W. Robledo. Infostat; Ed. Brujas: Córdoba, Argentina, **2008**.
[31] J. Hunter. *D Comput Sci Eng* **2007**, *9*(3), 90–95.